Article:
Zeng, P, Rainforth, WM and Stewart, TD (2017) Characterisation of the wear mechanisms in retrieved alumina-on-alumina total hip replacements. Wear, 376–37 (Part A). pp. 212-222. ISSN 0043-1648

https://doi.org/10.1016/j.wear.2016.11.045

Characterisation of the wear mechanisms in retrieved alumina-on-alumina total hip replacements

P Zeng[1], W M Rainforth[1] and T D Stewart[2] 1. Department of Materials Science and Engineering, University of Sheffield, Sheffield S1 3JD, UK 2. School of Mechanical Engineering, University of Leeds, Leeds LS2 9JT, UK

Abstract:

Due to their superior wear performance and biocompatibility compared to alternative polymer/metal prostheses, alumina-on-alumina total hip replacements (THRs) are extensively used for young and more active patients. However, the understanding of the wear mechanisms of alumina in vivo remains relatively poor, and there remains little quantitative understanding of the structural and chemical changes at the articulating surface. In the current study, the surface and sub-surface microstructures of retrieved in vivo alumina THRs are presented. Severe wear, also called stripe wear, was observed in all cases. The transition between the stripe wear and the mild wear was very sharp. Site-specific cross-section TEM specimens were prepared by Focused Ion Beam (FIB) at the stripe boundary region. The results suggest predominantly intergranular fracture occurred that was restricted to the outer layer of grains below the surface, with transgranular fracture also occurring in the stripe wear region. Cracking was believed to be initiated by extensive dislocation slip. A thin layer of hydroxide was also observed at the extreme surface of the mild wear region by aberration-corrected high resolution transmission electron microscopy (HRTEM). The wear mechanisms are discussed.

Keywords: alumina, high resolution transmission electron microscopy, focused ion beam, total hip replacement

1. Introduction

About 2% of people suffer hip problems and need a replacement hip joint. In the UK, at least 50,000 hip replacement surgeries are undertaken every year, and are highly successful in reducing the pain and disability of worn or damaged hip joints. Total hip replacement is one of the most successful applications of biomaterials, with joints commonly lasting more than 10 to 15 years [1, 2]. However, the long-term (> 15

years) performance of the THRs is only achieved in a small proportion of cases. With the increase of younger and high demand patients, as well as an increase in life expectancy, long-term (> 15 years) high performance THRs are increasingly required.

Since the 1960s, metal-on-polymer THRs are by far the most common artificial hip joints in the market [1]. However, due to the osteolysis (bone resorption) caused by polymer wear debris and component loosening, interest in alumina-on-alumina THRs continues to grow [3-5]. Additionally, alumina-on-alumina THRs show a higher survival rate than metal-on-polymer THRs for patients younger than 50 years old [6- 8]. With metal debris and ions release from CoCrMo alloys becoming a subject of intense interest due to the higher than expected failure rate of metal-on-metal hip replacements [9-11], alumina or alumina based ceramic THRs are increasingly used for young and more active patients.

Alumina-on-alumina THR was first introduced in the 1970s. However, early problems with the performance of the alumina-on-alumina THRs, such as a high fracture rate, restricted their development worldwide. This was mainly due to poor material quality and hip design. With the development of medical-grade alumina, especially the introduction of ISO 6474 alumina-on-alumina THRs now perform substantially better than the original 1st generation alumina. Although over 2.5 million alumina femoral heads and nearly 100,000 alumina acetabular cups have been implanted worldwide since the first introduction [12], the understanding of the wear mechanisms of alumina in vivo remains relatively poor. Since wear plays an important role in limiting the lifetime of artificial hip joints it is important to understand the wear mechanisms that operate in vivo in alumina-on-alumina THRs in detail.

In the wear of alumina-on-alumina THRs, most of the research undertaken to date has concentrated mainly on the wear performance of in vitro alumina hip prostheses. For the in vivo studies, the focus of attention has been on key performance indicators such as wear rate, survival rate, with virtually no focus on the microstructure and wear mechanisms. Similarly, for the in vitro testing, the output has often been simple parameters such as wear rate and general worn surface appearance. Only limited work on the microstructural evolution from wear of alumina-on-alumina THRs has been published [13-23]. A region of high wear, often referred to as ‘stripe’ wear, on the

surface of both alumina acetabular cups and femoral heads has been observed in retrieved in vivo alumina-on-alumina THRs [15]. However, wear mechanisms leading to this stripe wear are not clearly understood.

In the current study, surface morphology across the stripe wear of the retrieved in vivo alumina-on-alumina THRs was analysed by 3D optical microscopy and scanning electron microscopy (SEM). Sub-surface microstructure was studied using FIB, HRTEM and Electron Energy Loss Spectroscopy (EELS). Wear mechanisms leading to the stripe wear on the worn alumina-on-alumina THRs are discussed.

2. Experimental procedure

2.1 Materials

7 pairs of retrieved alumina-on-alumina THRs were investigated and the details of each pair are given in Table 1. An example of the retrieved in vivo alumina femoral head and acetabular cup are shown in Fig.1. The alumina ceramics used for operations were Biolox® alumina ceramic material with a mean grain size of 3.2 μm and a density of 3.95 g/cm^3.

Table 1 The dimension of stripe wear observed on the worn surface of retrieved in vivo alumina-on-alumina THRs investigated.

samples	Length of the stripe	Max. width of the stripe	Diameter of the hip prostheses	Notes
Head # 1	40.0 mm	12.0 mm	32 mm	2 years implanted,
Cup # 1	40.0 mm	12.0 mm	32 mm	failure by dislocation
Head # 2	75.4 mm	25.0 mm	32 mm	8 years implanted,
Cup # 2	50.2 mm	11.0 mm	32 mm	failure by loosening
Head # 3	38 mm	8 mm	38 mm	11 years implanted,
Cup # 3	67.0 mm	7.0 mm	38 mm	failure by loosening
Head # 4	51 mm	30.0 mm	32 mm	1 year implanted,
Cup # 4	50.2 mm	17.0 mm	32 mm	failure by loosening
Head # 5	26.0 mm	9.0 mm	38 mm	10 years implanted,
Cup # 5	39.8 mm	3 mm	38 mm	failure by loosening
Head # 6	32 mm	6 mm	32 mm	1 year implanted,
Cup # 6	33.5 mm	12 mm	32 mm	failure by migration
Head # 7	89.5 mm	23 mm	38 mm	12 years implanted,
Cup # 7	59.7 mm	10 mm	38 mm	failure by loosening

Fig.1 A pair of retrieved in vivo alumina femoral head and acetabular cup.

2.2 Characterisation

2.2.1 Surface characterisation

The worn surface of retrieved in vivo alumina-on-alumina THRs were first inspected by naked eye to locate the severe wear region, as shown in Table 1. The surface topography of the retrieved in vivo alumina femoral heads was examined by a 3D optical microscope (ContourGT, Bruker, UK).

Due to the difficulty and the size of the samples, it was not possible to investigate all the samples using SEM. Therefore, a pair of retrieved in vivo alumina-on-alumina THR was chosen carefully for further SEM investigation that was believed to be representative. The alumina THR chosen had been implanted for 12 years and failed by loosening (head # 7 and cup # 7 in Table 1). The material for the retrieved pair was 2nd generation Biolox with a mean grain size of 3.2 µm and density of 3.95 g/cm^3. The worn surfaces were analysed by SEM (Sirion, FEI Company, Netherlands) operating at 10 kV. The samples were coated with carbon before the investigation to avoid charging.

2.2.2 Sub-surface damage

Site-specific TEM samples were prepared by an in-situ focused ion beam (FIB) lift-out using a Quanta 200 3D FIB (FEI Company, Netherlands) equipped with an in-situ tungsten probe (Omniprobe, USA), as shown in Fig.2. A gold layer was sputtered (Emscope SC 500 A Sputter Coating Unit, UK) on the surface prior to FIB milling to label the original surface and avoid charging. For FIB processing, a 30 kV Ga^+ ion beam was used. Firstly, a carbon stripe was deposited onto the area of interest using a 0.3 nA beam current to prevent damage of the surface due to ion milling (Fig.2a).

Secondly, two trenches were milled on both sides of the carbon deposition using high beam currents (5 nA and 3 nA), as shown in Fig.2b. Thirdly, the TEM lamella was lifted out using the Omniprobe (Fig.2c) and attached to a TEM grid via carbon deposition (Fig.2d). Finally, the TEM lamella was further thinned from both sides with low beam currents (varied from 0.5 nA to 30 ρA) until it was electron transparent (< 50 nm), as shown in Fig.2e.

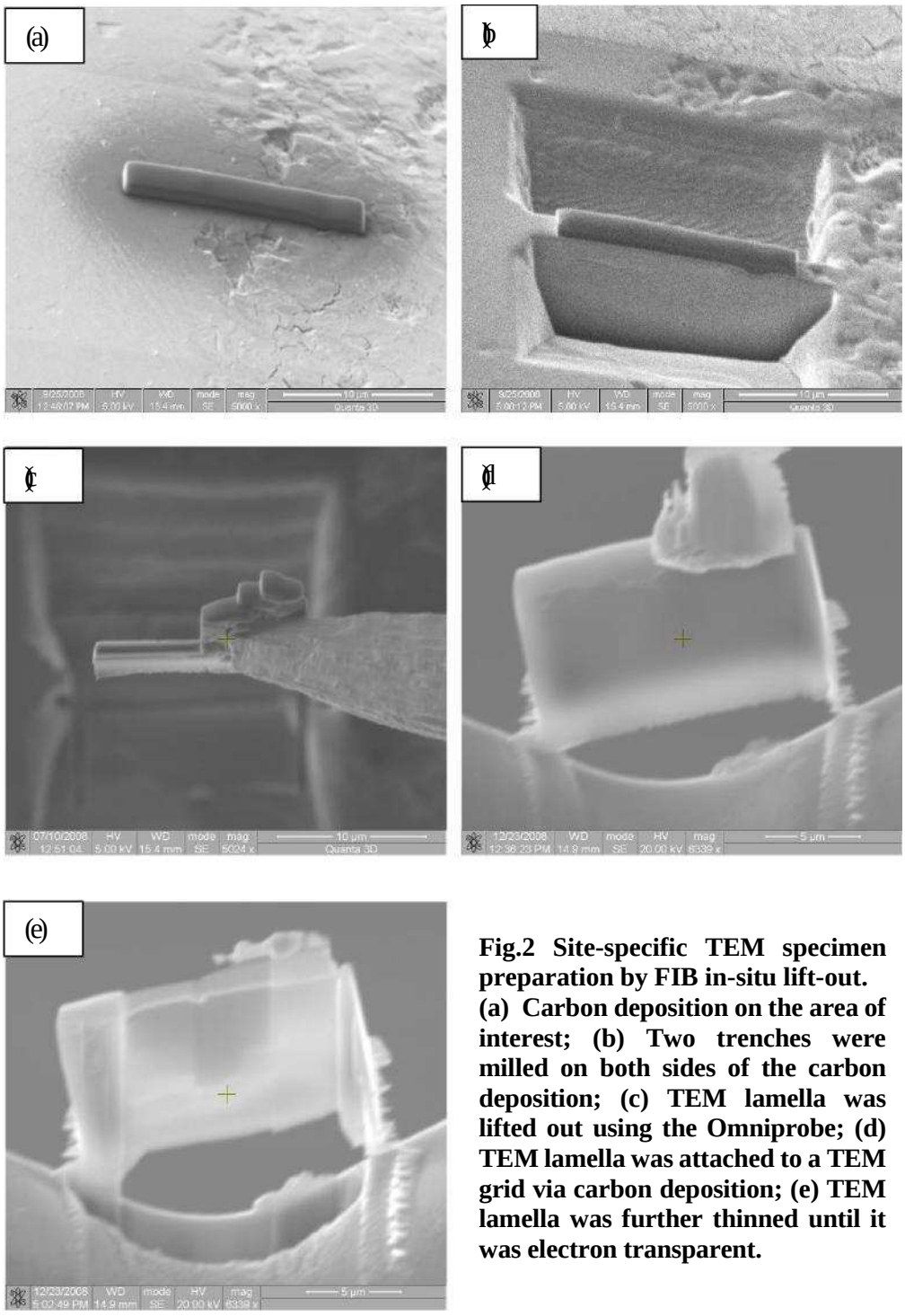

Fig.2 Site-specific TEM specimen preparation by FIB in-situ lift-out. (a) Carbon deposition on the area of interest; (b) Two trenches were milled on both sides of the carbon deposition; (c) TEM lamella was lifted out using the Omniprobe; (d) TEM lamella was attached to a TEM grid via carbon deposition; (e) TEM lamella was further thinned until it was electron transparent.

TEM investigation was carried out using various TEMs, including FEI Tecnai 20 (FEI, Netherlands), Jeol 2010F (JEOL, Japan) and Jeol R005 (JEOL, Japan), all operating at 200 kV. EELS (Gatan, USA) equipped on Jeol 2010F was employed to analyse the cross-section samples. EELS measurements were made in conventional TEM diffraction mode (image coupling to the spectrometer).

3. Results

3.1 Percentage of the stripe/severe wear on the retrieved in vivo alumina-on-alumina THRs

Table 1 summarises the dimension of the stripe wear on the worn surface of retrieved in vivo alumina-on-alumina THRs. Although they had failed for different reasons, all the retrieved in vivo alumina prostheses exhibited stripe wear on the surface. The length of the stripe ranged from 30 mm to 90 mm with maximum width ranging from 10 mm to 30 mm. Some prostheses showed a much larger area of severe wear than just a 'stripe' such that the area of severe wear almost covered the entire head, such as head # 4 (more than 80 %) in Table 1.

3.2 Surface characterisation of the retrieved alumina THRs

Four wear zones were observed on the worn surface of the simulated in vitro alumina THRs, which were, following the definitions used in our previous work [20-23]: mild wear zone, wear transition zone, stripe boundary zone and stripe wear zone. These four different wear zones were also seen on the worn surface of the retrieved in vivo alumina-on-alumina THRs, as shown in Fig.3 and Fig.4.

Fig. 3 shows SEM images of the worn surface from a retrieved in vivo alumina femoral head (head #7 in table 1). In the mild wear zone (Fig. 3a), parallel grooves due to the original polishing process could be observed. Wear debris was present on the surface inside the grooves. Evidence of surface deformation could also be observed, as arrows shown in Fig. 3a. In the wear transition zone, occasional surface pits due to grain pull out were seen in an otherwise smooth surface. Wear debris was widely observed, with some having a 'smeared' appearance, arrowed in Fig. 3b. A sharp boundary between the mild/transition wear and the stripe wear is shown in Fig. 3c. Intergranular fracture was observed along the stripe boundary. In the stripe wear zone, as shown in Fig. 3d, a rough surface was seen with clear fracture facets,

indicating predominantly intergranular fracture, but also some transgranular fracture. In addition, there were areas that had a 'smeared' appearance, presumably formed through the compaction of wear debris. Plastic deformation was also observed around the surface pits.

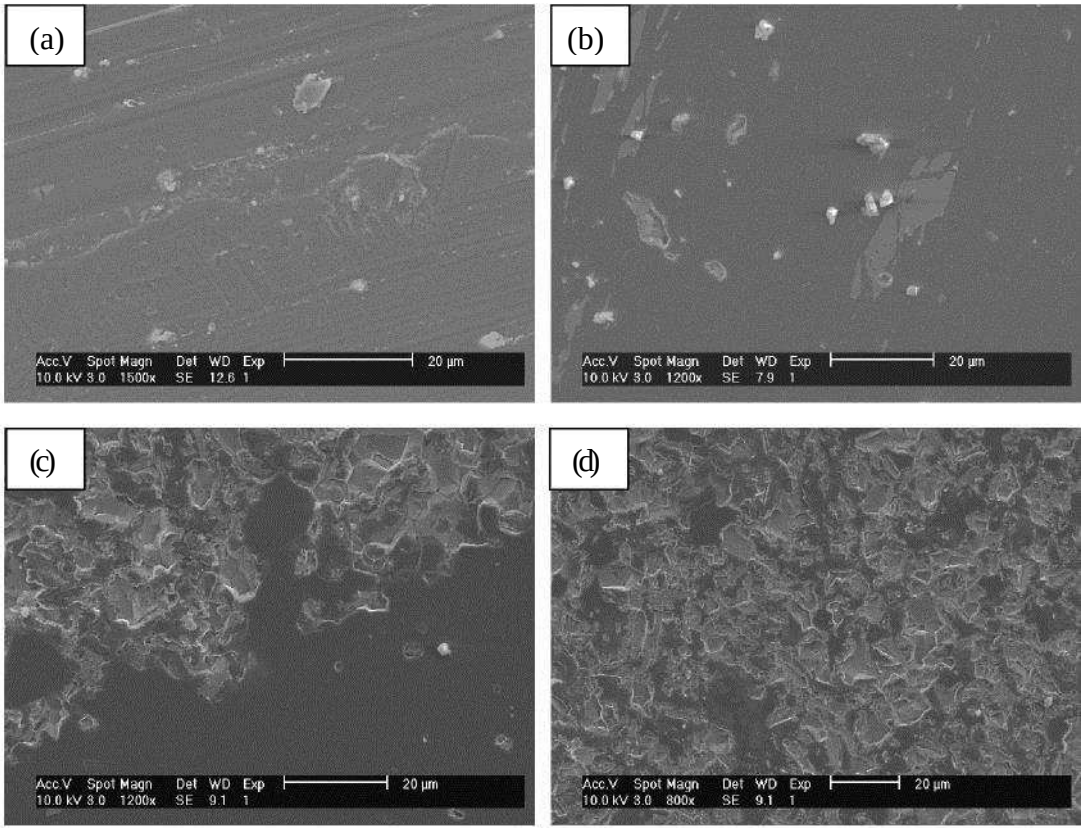

Fig. 3 SEM images of the retrieved in vivo alumina femoral head, showing (a) the mild wear zone, (b) the wear transition zone, (c) the stripe boundary zone and (d) the stripe wear zone. Arrows in (a) and (b) are explained in the text.

Fig. 4 shows the surface topography of the retrieved in vivo alumina femoral heads (representative of heads #1, #2, #3, #4 and #6 in table 1). Fig. 4a shows a low magnification image of the mild wear zone from the retrieved in vivo alumina femoral head, taken at the pole of the head. The parallel lines in the image were believed to be original polishing marks (note the concentric rings are an artefact caused by flattening the image of a strongly curved surface). A higher magnification image (Fig. 4b) shows the original polishing marks with some mechanical damage that had left small gouges in the surface, together with occasional wear debris standing proud of the surface.

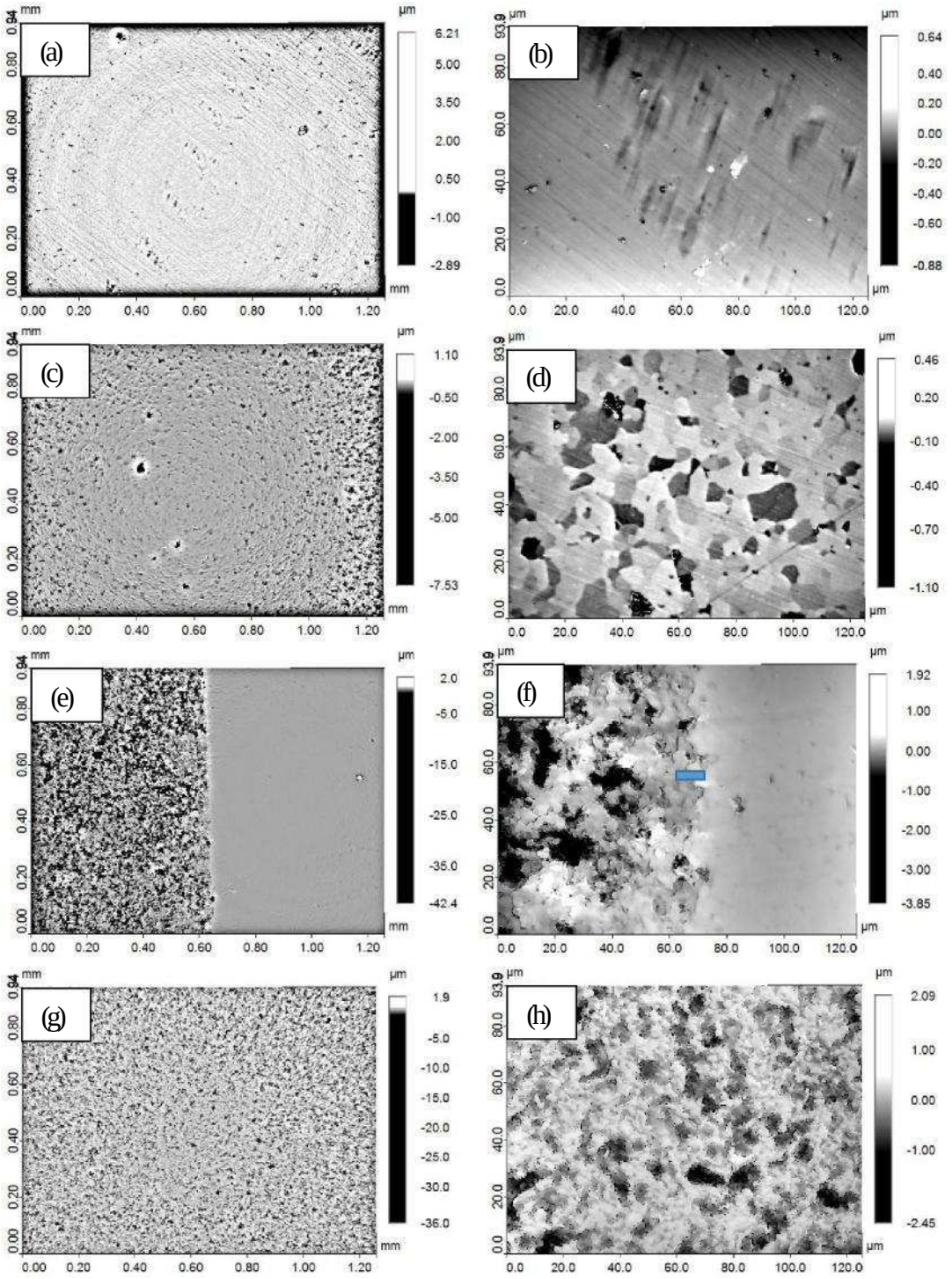

Fig.4 Surface topography of four wear zones of the retrieved in vivo alumina femoral head. The mild wear zone (a) and the magnified image (b); the wear transition zone (c) and the magnified image (d); the stripe boundary zone (e) and the magnified image (f); the stripe wear zone (g) and the magnified image (h). The rectangle in (f) indicates the location of TEM cross-section.

In the wear transition zone, a pitted surface could be seen (Fig. 4c). A magnified image (Fig. 4d) revealed grain relief on the surface, indicating the wear rate differed from grain to grain. An abrupt boundary could be seen at the boundary to the stripe

boundary, as shown in Fig. 4e. Dramatic changes were seen, with surface pitting due to grain pull out visible along the stripe boundary (Fig. 4f). The location of the TEM cross-section is shown in Fig. 4f, which is discussed later. In the stripe wear zone, a highly pitted surface was observed (Fig. 4g). Magnified image (Fig. 4h) shows grain pull out and smearing of the wear debris.

The surface profile of the alumina femoral heads in different wear zones is shown in Fig.5 (representative of heads #1, #2, #3, #4 and #6 in table 1). In the mild wear zone (Fig. 5a), a smooth surface with occasional peaks (which were believed to be wear debris) could be seen. A mean roughness (Ra) of 59 nm was measured in this region. Fig. 5b gives a surface profile in the wear transition zone, indicating grain relief, i.e. individual grains were wearing at different rates. Interestingly, a mean roughness of 32 nm was measured, which indicates a smooth surface in the wear transition zone, in the agreement with the SEM observations. In the stripe boundary zone (Fig. 5c), an abrupt change from mild/transition to severe wear could be seen. An Ra roughness of 250 nm was measured. Fig. 5d, which shows the surface profile in the stripe wear zone, which exhibited a rough surface with a measured Ra of 251 nm.

In addition to Ra, the skewness (Ssk) and kurtosis (Sku) were measured in the various wear zones, the results of which are presented in Table 2. The skewness is a measure of the degree of asymmetry of the surface height distribution about the mean plane and kurtosis is a measure of the sharpness of the peaks. Ssk and Sku can be evaluated as:

$$Ssk = \frac{1}{sq^3} \iint a\,(z(x,y))^3 dxdy$$

$$Sku = \frac{1}{sq^4} \iint a\,(z(x,y))^4 dxdy$$

A negative Ssk could be seen in all regions, indicating the dominance of valleys in the profile, which of course is associated with grain pull-out. A value of Sku > 3 is normally taken to indicate inordinately high peaks or deep valleys. The values of Sku in Table 2 indicate inordinately deep valleys in all cases. However, these were surprisingly larger for mild and wear transition zones, perhaps because in the wear transition zone and the stripe wear region the valleys had been filled by wear debris.

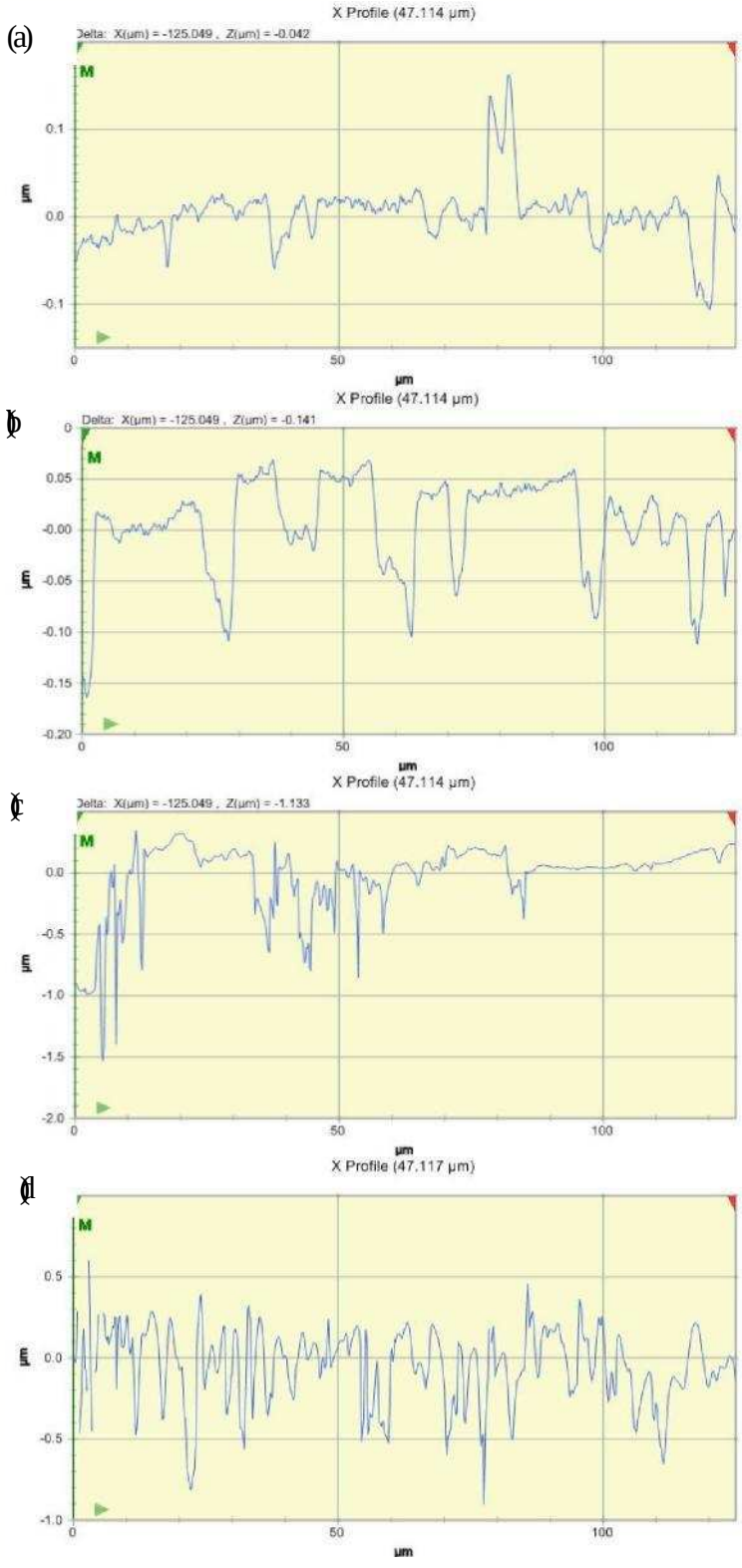

Fig.5 Surface profiles of the retrieved in vivo alumina femoral head in the mild wear zone (a), the wear transition zone (b), the stripe boundary zone (c) and the stripe wear zone (d).

The mean roughness was also measured by 3D optical microscopy according to the geometric location on the surface, as shown in Table 3. In the mild/transition wear

zone, the mean roughness of 7- 64 nm was observed on the retrieved alumina femoral heads. However, on the pole or equator of the retrieved alumina heads, an increasing mean roughness could be seen. In other words, increased roughness tended to appear on the pole or near the equator of the femoral heads, which also corresponded to the severe wear region. Therefore, it could be concluded that the severe wear regions are related to the impact caused by edge loading.

Table 2 3D surface roughness parameter values, skewness, Ssk and kutosis, Sku, in various wear zones.

Wear zone	Ssk	Sku
Mild wear	-0.4	14.0
Wear transition	-2.0	16.3
Stripe boundary	-1.9	9.3
Stripe wear	-1.2	5.2

Table 3 The mean roughness (Ra) of different regions on the worn surface of retrieved in vivo alumina acetabular head, measured by 3D optical microscopy.

Sample	Pole	Mild/transition	Equator
Head # 1	445 nm	34 nm	705 nm
Head # 2	127 nm	34 nm	217 nm
Head # 3	56 nm	64 nm	180 nm
Head # 4	258 nm	7 nm	174 nm
Head # 6	37 nm	40 nm	241 nm

3.3 Sub-surface characterisation of the retrieved in vivo alumina THRs

Fig. 6 shows TEM images of the site-specific cross-section of a retrieved in vivo alumina femoral head (head # 7 in Table 1) from the stripe boundary zone (as indicated in Fig. 4f). Fig. 6a is a plan-view with stripe wear zone on the left side and mild/transition wear zone on the right side, as indicated. A high dislocation density could be seen in the surface grains in both wear zones. It is important to note that the dislocation slip was limited in the outermost grains and was not observed in the grains below. Intergranular fracture was seen between grains in the stripe wear zone and the mild/transition wear zone, as shown in Fig. 6b. In the stripe wear zone, not only intergranular fracture, but also transgranular fracture could be observed (Fig. 6c). The inset diffraction pattern from the top region indicated substantial arcing in the diffraction spots for a particular plane, typical of misorientations arising from high dislocation density sub grain boundaries. The difference between the stripe wear zone and the mild/transition zone appeared to be that in the former, grains had been lost

from the surface from fracture, while in the latter, cracking had occurred, but it had not yet led to loss of surface grains. However, given the amount of damage observed in the mild/transition region, it is clear that grain pull out was imminent.

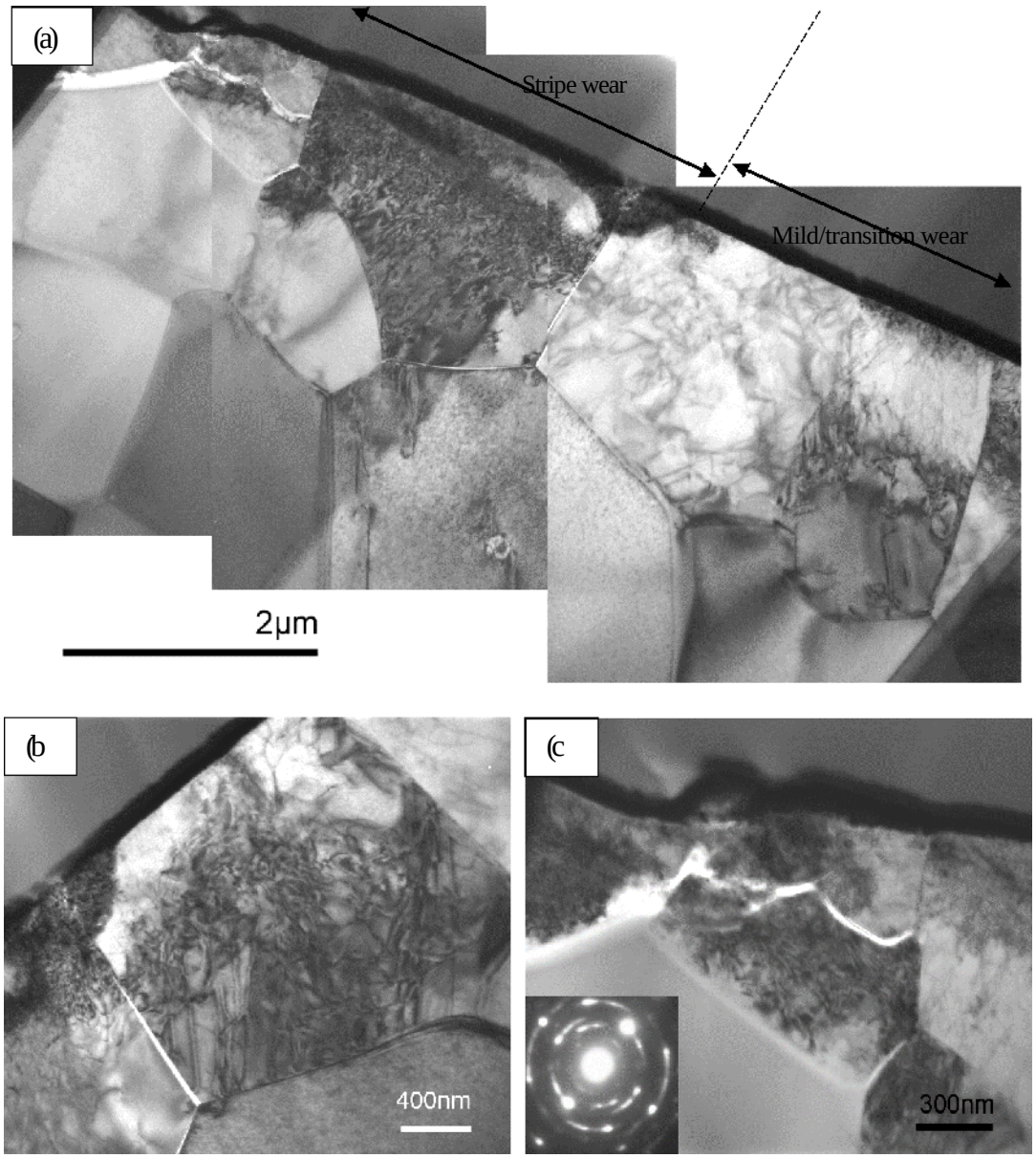

Fig.6 Site-specific TEM cross-section of the retrieved in vivo alumina femoral head from the stripe boundary zone. (a) A plan-view; (b) intergranular fracture between grains in the mild/transition wear zone and the stripe wear zone; and (c) intergranular fracture and transgranular fracture in the stripe wear zone, with diffraction pattern from the top surface inset.

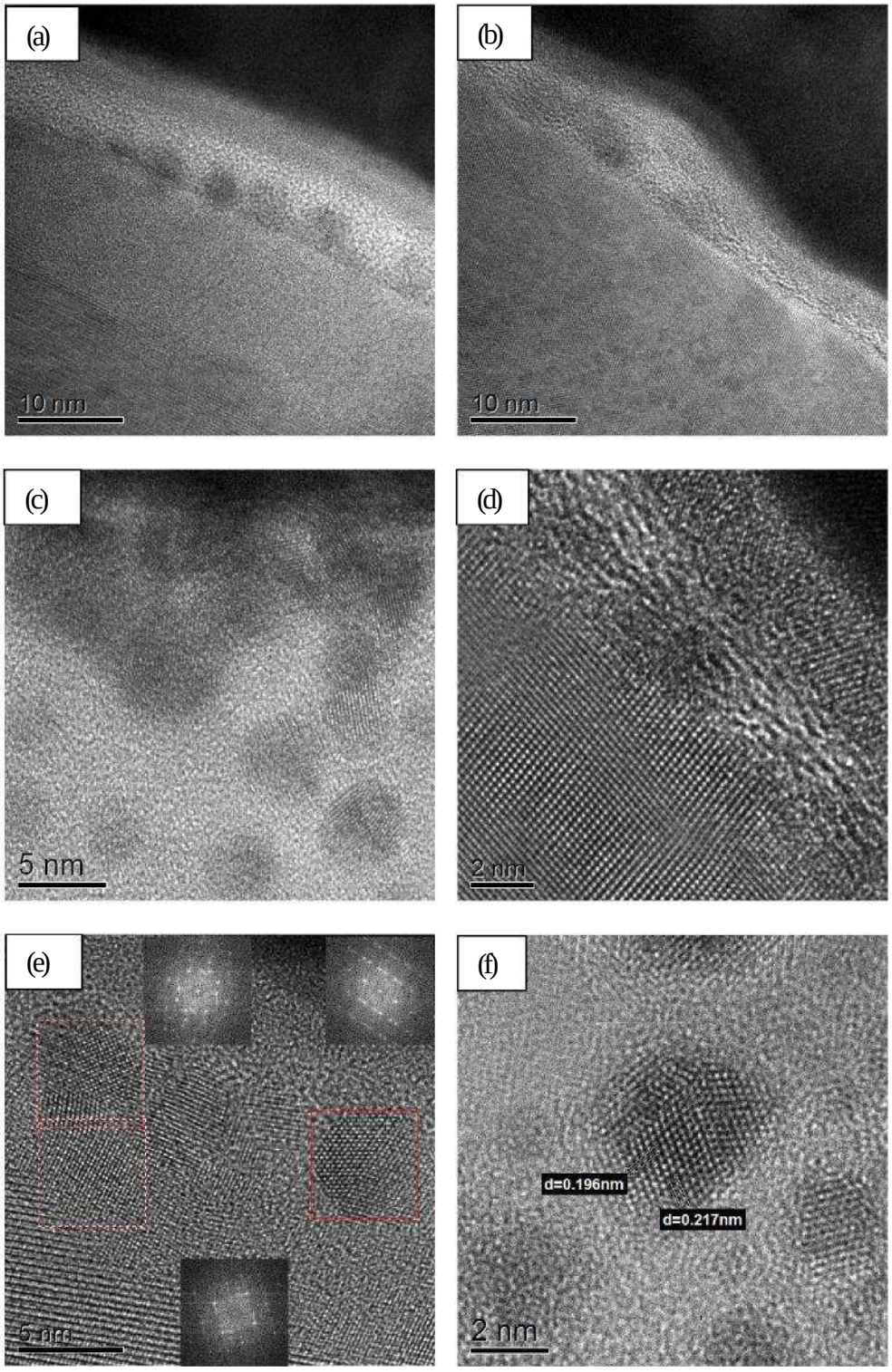

Fig.7 HRTEM images of the cross-section from the stripe wear zone in the mild/transition side. (a) In the mild wear region shows a thin amorphous layer with nano-crystals embedded, as well as a thin hydroxide layer. (b) In the wear transition region shows only a thin amorphous layer with nano-crystals embedded. (c) A thick amorphous layer with nano-crystals ranged from 2-5 nm. (d) A thin amorphous layer less than 2 nm. (e) Detail of nano-crystals in the amorphous layer, insets are FFT of selected nano-crystals. (f) Detail of a nano-crystal in the amorphous layer with d-spacing of 0.196 nm and 0.217 nm, respectively.

High resolution TEM (HRTEM) images of the site-specific TEM cross-section from the stripe boundary zone are shown in Fig. 7 and Fig. 8. HRTEM images of the top surface in the mild wear zone are shown in Fig.7. An amorphous layer of about 9 nm thick was seen, Fig. 7a, that was embedded with nano-crystals ranged from 2 nm to 5 nm in diameter. Below this, a layer ~ 10 nm thick was observed, that clearly had a different structure to that of the substrate. Fast Fourier Transfer (FFT) of the HRTEM image of this region suggested that the layer might be caused by the formation of aluminium hydroxide.

Fig. 7b shows the surface structure from a region of the wear transition zone. A thinner (~2 nm) amorphous layer was observed with no suggestion of aluminium hydroxide being present. However, nano-crystal particles were observed embedded in the amorphous layer. A thicker (~20 nm) amorphous layer could also be seen, as shown in Fig. 7c. Again, nano-crystals in the range of 2 nm to 5 nm were observed. Fig. 7d shows a HRTEM image showing a thin amorphous layer (< 2 nm) on the worn surface. Fig. 7e and f give magnified images of the nano-crystals observed. FFT of the three chosen nano-particles are shown in the inset, indicating two of the three particles were alumina particles with d spacing measured of 0.196 nm and 0.217 nm, representing (1011) and (0001) planes of alumina respectively (while the third was a gold particle from gold coating). Furthermore, d spacing of a nano-particle was measured, as indicated in Fig. 7f. Therefore, it can be concluded that the nano-particles in the amorphous layer were mainly alumina nano-crystals wear debris particles.

Fig. 8 gives HRTEM images of the top surface in the stripe wear zone. Compared with the observation in the mild/transition wear zone, a thinner amorphous layer was seen (~ 2 nm to 5 nm). A mixture of alumina nano-crystals and gold nano-particles could be seen by FFT and d spacing measurement (Fig. 8b-d).

Fig. 9 compares three normalised electron energy loss (EEL) spectra taken from the amorphous layer, the amorphous layer close to alumina matrix and the alumina matrix. Ca $L_{2,3}$ –edges were observed in the amorphous layer, suggesting the amorphous layer was the result of the tribochemical reaction between the body fluid and the alumina

surface. The O K-edge was seen in all the spectra, however, O K-edge near edge structure characteristic of alumina was only seen in the alumina itself.

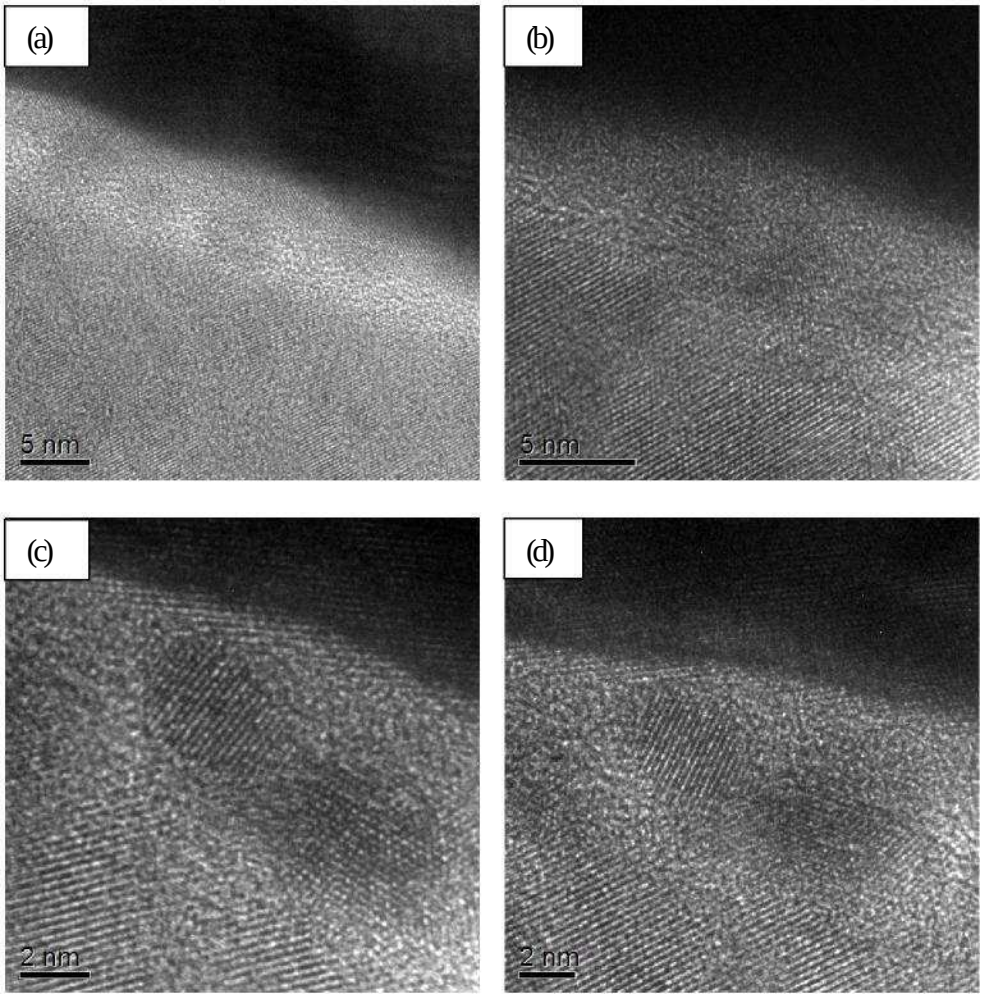

Fig. 8 HRTEM images of the cross-section from the stripe wear zone in the stripe wear side. (a) A thin amorphous layer is shown. (b)-(d) show a mix of alumina nano-crystals and gold nano-crystals.

Fig.9 Normalised experimental EEL spectra from the amorphous layer (bottom), the amorphous layer close to alumina matrix (middle) and alumina matrix (top).

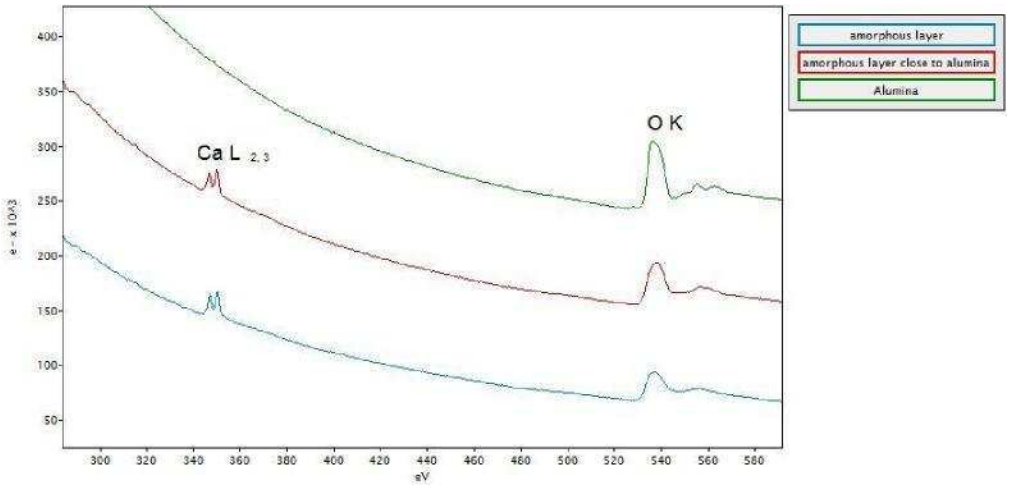
amorphous layer
amorphous layer close to alumina
Alumina
O K
Ca L 2,3
e⁻ x 10^3
eV

4. Discussion

4.1 Wear zones

Four wear zones were observed from the retrieved in vivo alumina femoral heads and acetabular cups, namely: the mild wear zone, the wear transition zone, the stripe boundary zone and the stripe wear zone, which in consistent with our previous work on the simulated in vitro alumina THRs [20-23]. However, the boundary between the mild wear zone and the wear transition zone was less obvious on the worn surface of the retrieved in vivo alumina THRs compared with the observation on the worn surface of the simulated in vitro alumina THRs. In most cases, a mild/transition wear zone was observed.

The results are broadly similar to those reported by Nevelos et al. [14-16], who investigated retrieved in vivo alumina THRs, and defined three regions according to the wear pattern observed; namely, low wear, stripe wear and severe wear. Likewise, Yamamoto et al. [17-21], classified five regions based on wear severity. Such classification has also been used by Manka et al. [24], who showed that the wear zones were broadly similar in retrieved alumina THRs and those simulated tested with microseparation.

The results are also in agreement with Affatoto et al. [25] who investigated six retrieved alumina hip implants for severe damage after a mean follow-up of 13 years and mapped the wear pattern as: occasional pits in an otherwise smooth surface; large-scale loss of grains, probably due to a fracture mechanism; a transition zone from low to severe wear, corresponding to the transition from lapped to the abraded zone.

It is important to note that the regions exhibiting increased roughness tended to be on the pole or near the equator of the femoral head (Table 3), where severe wear was highly likely to occur. These results suggest that high impact occurred on the top or near the equator of the femoral head, which resulted in severe wear, was a result of edge loading due to microseparation [26]. Thus, the stripe wear region appears to be associated with edge loading in these cases.

Perhaps not surprisingly, the skewness of the surface roughness profiles indicated that valleys dominated the profile. Such values are known to result in lower friction [27]. It was interesting to see that higher values of the kurtosis were observed for the mild and wear transition regions than for the stripe and stripe boundary regions. The valleys in each case were formed by grain pull out, but SEM suggested that the stripe wear regions contained extensive wear debris in them, which presumably reduced the value of the kurtosis.

4.2 Wear Mechanisms

Plastic deformation by dislocation slip is believed to have contributed to the wear of alumina-on-alumina THRs, however, no direct observation of this mechanism has been reported before. In the current study, we have shown for the first time that plastic deformation occurred on the worn surface of retrieved in vivo alumina-onalumina THRs using site-specific TEM. Indeed, plastic deformation was widely seen on the worn surface of retrieved alumina-on-alumina THRs, even in the mild wear zone (as shown in Fig. 3a). The high dislocation activity under the worn surface (Fig. 6), in both severe wear and mild wear regions, was restricted to the outer alumina grain in all cases, with the grains further below the surface largely dislocation free, as shown in Fig. 6. Even in the stripe wear zone where severe wear was observed, the plastic deformation was limited in the outermost grains, as shown in Fig. 6a and Fig. 6c. This is in agreement with Barceinas-Sanchez and Rainforth [27] who observed dislocation activity distributed heterogeneously throughout the surface grains, when polycrystalline α-alumina was worn against Mg-partially stabilized zirconia using water lubrication.

Tribochemical reactions are believed to control the mild wear of alumina and forms hydroxide layers [29, 30]. Rainforth [31] concluded that the wear rate of ceramic-on-ceramic wear was determined by the rate of hydration of the surface, the removal of the hydrated film, and the damage caused by the film as a 3-body abrasive. Additionally, the amorphous wear debris rather than crystalline wear debris was observed at the sliding surface of ceramics that was believed to be hydrated phase. Fischer et al. [32] studied the sliding wear of alumina and observed thin hydroxide layers, which can act as lubricants. In addition, roll wear debris was observed as a result of removal of the layer. However, the amorphous wear debris was not seen in

the current work and our previous work [23] on simulated in vitro alumina hip prostheses, even though a thin amorphous layer (~ 2 nm to 5 nm) was widely observed on the surface, as shown in Fig. 7 and Fig. 8. In addition, a thin hydroxide layer (~ 10 nm) was directly observed by HRTEM in the mild wear zone (Fig. 7a). EEL spectra (Fig. 9) showed the existence of Ca $L_{3,2}$ edges together with O K edge in the amorphous layer, indicating the layer was the product of tribochemical reaction between alumina and the body fluid. Therefore, tribochemical wear did happen in the wear of alumina-on-alumina THRs, but was restricted to the mild wear regions and was clearly not the main reason causing the failure of the components.

The current results suggest that high wear associated with fracture of the surface grains was the dominant wear mechanism initiating the failure of the alumina-onalumina THRs. Barceinas-Sanchez and Rainforth [28] studied the wear of alumina in water lubrication environment, indicating that grain boundary microcracking arises directly from dislocation pile-ups at grain boundaries and proposed the following sequence: 1) the local contact stresses increase because of a reduced real contact area as a result of the differential wear between grains (grain relief). 2) The increase in the contact stresses produces dislocation flow and cracks initiate at the grain boundaries due to dislocation pile-ups. 3) Grain boundary cracking leads to the formation of a wear particle. 4) The liberated wear particle acts as a third-body abrasive. 5) At some point the dislocation and microcrack density reach a critical value that, in combination with residual thermal stresses and asperity contact stresses, promote intergranular fracture at the surface and a catastrophic increase in wear rate. In the case of aluminaon-alumina THRs, because of the design of the femoral head and the actabular cup, the entire articulating surface is in contact, resulting in deformation anywhere on the surface, as seen in Fig. 3 and Fig. 6. However, the contact stresses here are probably too low to cause high wear. However, edge loading due to microseparation increases the contact stresses in certain areas, particularly at the equator or the pole of the alumina femoral head, leading to crack initiation at the grain boundaries due to dislocation pile-ups. The nature of the loading explains the sharp boundary observed between the stripe wear and surrounding regions (Fig. 3c, Fig. 4e, Fig. 4f and Fig. 6a). Intergranular fracture at the surface leads to the formation of wear particles with crystalline structure (Fig. 7 and Fig. 8). The liberated wear particles are embedded in the amorphous tribo-layer and presumably can act as third-body abrasives (Fig. 7 and

Fig. 8). In the severe wear region, the dislocation and microcrack density reach a critical value, promoting intergranular and transgranular fracture at the surface.

5. Conclusions

1. Four wear zones were observed from retrieved in vivo alumina-on-alumina THRs, namely: mild wear zone, wear transition zone, stripe boundary zone and stripe wear zone.
2. Site-specific TEM cross-section samples of retrieved in vivo alumina femoral heads were prepared by FIB for the first time.
3. Plastic deformation due to dislocation activity was distributed throughout the worn surface and concentrates in the outermost grain. Dislocation pile-ups at grain boundaries resulted in grain boundary cracking, which resulted in intergranular fracture.
4. The dislocation and microcrack density reach a critical value, at which point, intergranular and transgranular fracture was promoted at the surface, leading to the formation of the stripe wear region. Therefore, surface plastic deformation was a key step in the formation of stripe wear.
5. Fracture, tribochemical wear and three-body abrasive wear contributed to the wear of retrieved in vivo alumina-on-alumina THRs, however, intergranular and transgranular fracture in the stripe wear region was the dominant wear mechanism.

References:

[1] D. Dowson, New joints for the millennium: wear control in total replacement hip joints. Proc Instn Mech Engrs: Part H. 215 (2001): 335-358.

[2] J. D'Antonio, W. Capello, M. Manley, B. Bierbaum, New experience with alumina-on-alumina ceramic bearings for total hip arthroplasty. J Arthroplasty. 17 (2002): 390-397.

[3] H.J. Früh, G. Willmann, Tribological investigations of the wear couple alumina-CFRP for total hip replacement. Biomaterials. 19 (1997): 1145-1150.

[4] M. Slonaker, T. Goswami, Review of wear mechanisms in hip implants: Paper II- ceramics IG004712. Materials & design. 25 (2004): 395-405.

[5] T.R. Yoon, S.M. Rowe, S.T. Jung, K.J. Seon, W.J. Maloney, Osteolysis in association with a total hip arthroplasty with ceramic bearing surface. J Bone Joint Surg 80A (1998): 1459-1468.

[6] L. Sedel, M. Hamadouche, P. Bizot, R. Nizard, Long term data concerning the use of alumina on alumina bearings in total hip replacements. Key Engineering Materials, 240-242 (2003): 769-772.

[7] H.J. Yoon, J.J. Yoo, K.S. Yoon, K.H. Koo, H.J. Kim, Alumina-on-alumina THA performed in patients younger than 30 years: a 10-year minimum follow up study. Clin Orthop Relat Res 470 (2012): 3530-3536. DOI 10.1007/s11999-012-2493-2.
[8] J.J. Yoo, P.W. Yoon, Y.K. Lee, K.H. Koo, K.S. Yoon, H.J. Kim, Revision total hip arthroplasty using an alumina-on-alumina bearing surface in patients with osteolysis. J. Arthroplasty. 28 (2013): 132-138. DOI 10.1016/j.arth.2012.04.030.
[9] A.J. Smith, P. Dieppe, K. Vernon, M. Porter, A.W. Blom, Failure rates of stemmed metal-on-metal hip replacements: analysis of data from the national joint registry of England and Wales. Lancet 380 (2012) 1759-1766.
[10] R.N. De Steiger, J.R. Hang, L.N. Miller, S.E. Graves, D.C. Davidson, Five-year results of the ASR XLA acetabular system and the ASR hip resurfacing system: an analysis from the Australian orthopaedic association national joint replacement registry. J. Bone Jt. Surg. Am. 93 (2011) 2287-2293.
[11] F.W. Chan, J.D. Bobyn, J.B. Medley, J.J. Krygier, S. Yue, M. Tanzer, Engineering issues and wear performance of metal on metal hip implants. Clin. Orthop. Relat. Res. 333 (1996) 96-107.
[12] G. Willmann, Ceramic femoral head retrieval data. Clin. Orthop. 37 (2000): 22-28.
[13] A. Walter, W. Plitz, Wear of retrieved alumina-ceramic hip joints. Ceramics in surgery, edit by Vincenzini, (1983): 253-259. Elsevier: Amsterdam.
[14] A.B. Nevelos, P.A. Evans, P. Harrison, M. Rainforth, Examination of alumina ceramic components from total hip arthroplasties. Proc Instn Mech Engrs 207 (1993): 155-162.
[15] J. Nevelos, E. Ingham, C. Doyle, R. Streicher, A. Nevelos, W. Walter, J. Fisher, Microseparation of the centres of alumina-alumina artificial hip joints during simulator testing produces clinically relevant wear rates and patterns. J Arthroplasty, 15 (2000): 793-795.
[16] J.E. Nevelos, F. Prudhommeaux, M. Hamadouche, C. Doyle, E. Ingham, A. Meunier, A.B. Nevelos, L. Sedel, J. Fisher, Comparative analysis of two different types of alumina-alumina hip prosthesis retrieved for aseptic loosening. J Bone Joint Surg Br 83B (2001): 598-603.
[17] T. Yamamoto, M. Saito, M. Ueno, T. Hananouchi, Y. Tokugawa, K. Yonenobu, Wear analysis of retrieved ceramic-on-ceramic articulations in total hip arthroplasty: femoral head makes contact with the rim of the socket outside of the bearing surface. J Biomed Mater Res Part B-Applied Biomat, 73B (2005): 301-307.
[18] T. Shishido, K. Yamamoto, I.C. Clarke, T. Masaoka, M. Manaka, T. Tateiwa, Comparison of the results of a simulator study and retrieval implants in ceramic THA. Bioceramics 18 (2006): 1277-1280.
[19] T. Shishido, K. Yamamoto, S. Tanaka, T. Masaoka, I.C. Clarke, P. Williams, A study for a retieved implant of ceramic-on-ceramic total hip arthroplasty. J Arthroplasty. 21 (2006): 294-298.
[20] P. Zeng, B.J. Inkson, W.M Rainforth, Characterisation of alumina hip-joint wear by FIB microscopy. J Phys: Conf Ser 26 (2006): 343-346. DOI 10.1088/1742-6596/26/1/083.
[21] P. Zeng, B.J. Inkson, W. M. Rainforth, T. Stewart, 3D surface reconstruction and FIB microscopy of worn alumina hip prostheses. J Phys: Conf Ser 126 (2008): 012044. DOI 10.1088/1742-6596/126/1/012044.
[22] P. Zeng, W.M. Rainforth, B.J. Inkson, T.D. Stewart, Characterisation of worn alumina hip replacement prostheses. J Biomed Mater Rese Part B. 100B (2012): 121-132. DOI 10.1002/jbm.b.31929.
[23] P. Zeng, W.M. Rainforth, B.J. Inkson, T.D. Stewart, Transmission electron microscopy analysis of worn alumina hip replacement prostheses. Acta Mater 60 (2012): 2061-2072. DOI 10.1016/j.actamat.2012.01.009.

[24] M. Manaka, I.C. Clarke, K. Yamamoto, T. Shishido, A. Gustafson, A. Imakiire, Stripe wear rates in alumina THR-comparison of microseparation simulator study with retrieved implants. J Biomed Mater Res Part B-Applied Biomat, 69B (2004): 149-157.
[25] S. Affatato, P. Taddei, S. Carmignato, E. Modena, A. Toni, Severe damage of aluminaon-alumina hip implants: wear assessment at a microscopic level. J Euro Ceram Soc 32 (2012): 3647-3657. DOI 10.1016/j.jeurceramsoc.2012.05.023.
[26] W.M. Rainforth, P. Zeng, L. Ma, A. Nogiwa-Valdez, T. Stewart, Dynamic surface microstructural changes during tribological contact that determine the wear behaviour of hip prostheses: metals and ceramics. Faraday Discuss., 156 (2012): 41-57. DOI 10.1039/c2fd00002d.
[27] M. Sedlacek, B. Podgornik, J. Vizintin. Correlation between standard roughness parameters skewness and kurtosis and tribological behaviour of contact surfaces. Tribo Int 48 (2012): 102-112. DOI 10.1016/j.triboint.2011.11.008.
[28] J.D.O. Barceinas-Sanchez, W.M. Rainforth. On the role of plastic deformation during the mild wear of alumina. Acta Mater 46 (1998): 6475-6483.
[29] R.S. Gate, S.M. Hsu, E.E. Klaus. Tribochemical mechanism of alumina with water. J Soc Tribologists and lubrication engineers 32 (1989): 357-369.
[30] M.G. Gee, The formation of aluminium hydroxide in the sliding wear of alumina. Wear 153 (1992): 201-227.
[31] W.M. Rainforth, The sliding wear of ceramics. Ceramics International 22 (1996): 368-372.
[32] T.E. Fischer, Z. Zhu, H. Kim, D.S. Shin, Genesis and role of wear debris in sliding wear of ceramics. Wear 245 (2000): 53-60.